VNU Journal of Science: Mathematics - Physics
Journal homepage: https://js.vnu.edu.vn/MaP

Original Article

Effect of Annealing Temperatures on Structural and Luminescence Properties of SnO_2 Nanoparticles

Trinh Thi Loan*, Vu Hoang Huong

VNU University of Science, 334 Nguyen Trai, Thanh Xuan, Hanoi, Vietnam

Received 6th June 2025
Revised 21st June 2025; Accepted 30th September 2025

Abstract: This study aims to understand the structural and photoluminescence properties of SnO_2 synthesized via the facile sol–gel method by systematically varying annealing temperatures. X-ray diffraction (XRD) analysis reveals that all samples possess a polycrystalline single-phase tetragonal rutile structure with no detectable impurity phases. Both the crystallite size and crystalline quality of the samples increase with rising annealing temperatures. Raman spectroscopy demonstrates the presence of forbidden Raman and IR-active modes in SnO_2 nanoparticles. The positions and intensities of the Raman peaks are significantly influenced by the annealing temperature, which correlates with variations in crystallite size and crystalline quality of the synthesized materials. Additionally, photoluminescence (PL) spectra exhibit peaks in both the ultraviolet (UV) and visible regions. The UV emission peaks arise from electron recombination near the band gap, while the visible emission peaks are attributed to oxygen vacancies (V_O^0, V_O^+, V_O^{++}) and tin interstitials. This research provides valuable foundational knowledge that will support future studies on SnO_2.

Keywords: Sol-gel, SnO_2 nanoparticles, annealing temperature, Raman, luminescence.

1. Introduction

In recent years, many researchers have focused on synthesizing SnO_2 nanomaterials in various sizes and shapes to investigate their unique properties [1]. Tin dioxide is widely studied because it is chemically stable, transparent to light, and an excellent conductor of electricity [2, 3]. These properties make SnO_2 useful in several applications, including batteries [4], dye-sensitized solar cells [5], photocatalysis [6], transparent electrodes [7], and gas sensors [8]. The properties of SnO_2, such as band gap, crystal structure, morphology, and defects, can be tailored by adjusting the synthesis conditions,

* Corresponding author.
E-mail address: loan.trinhthi@gmail.com

https//doi.org/10.25073/2588-1124/vnumap.5028

including temperature, precursor materials, and solvents used [9]. In this study, SnO_2 nanoparticles were synthesized using the sol–gel method with $SnCl_2$ as the precursor material, without adding any capping agents or surfactants. We investigated how the size of the nanoparticles affects their light emission properties. Understanding these photoluminescence properties helps us learn more about the optical behavior of SnO_2 nanomaterials and improves their use in optical devices. The results of this study provide important foundational knowledge for future research and applications of SnO_2 in various technological fields.

2. Experimental

SnO_2 nanoparticles were synthesized using the sol-gel method. The precursor, $SnCl_2.2H_2O$ was dissolved in 30 mL C_2H_5OH with constant stirring. Next, the 10 ml ethylen glycol was added to the mixture solution under vigorous stirring. The solution was then heated at 100 °C while stirring until a transparent gel was formed, then dried at 100 °C for 24 h. The dried product was annealed at tempertures of 400, 600, 800 and 1100 °C for 3 hours.

The crystalline structure of SnO_2 nanoparticles was studied by an Empyrean X-ray diffractometer (XRD), using Cu-Kα1 irradiation (λ = 1.54056 Å). Raman spectra were obatained using a micro-Raman spectrophotometer LabRAM HR 800 (HORIBA JobinYvon) with a 632.8 nm excited wavelength. The morphologies of the samples were examined using a transmission electron microscope (TEM, JEOL/JEM 1010). Photoluminescence (PL) and photoluminescence excitation (PLE) spectra were recorded at room temperature using a Fluorolog FL3-22 spectrofluorometer (Jobin Yvon Spex) with a 450 W xenon lamp as the excitation source.

3. Results and Discussion

3.1. Structure Characterization

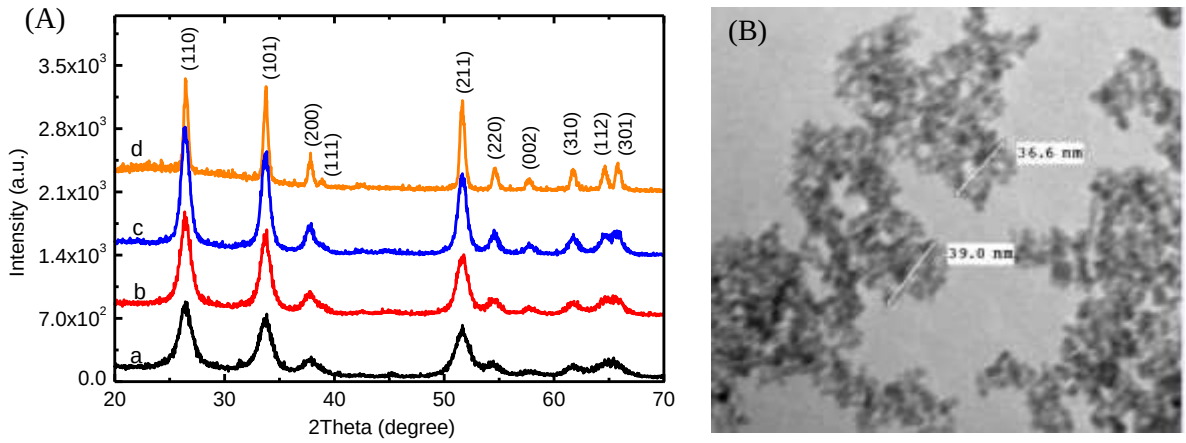

Figure 1. (A) XRD patterns of SnO_2 samples at different annealing temperatures: a- 400 °C, b- 600 °C, c- 800 °C, d- 1100 °C; (B) FESEM image of SnO_2 sample annealed at 600 °C.

The XRD patterns of SnO_2 samples annealed at temperatures of 400, 600, 800 and 1100 °C are presented in Figure 1(A). All the samples have XRD peaks at 2θ of ~ 26.44°, 33.70°, 37.81°, 39.98°,

51.67°, 54.51°, 57.66°, 61.75°, 64.59° and 65.40°. These peaks correspond respectively to the (110), (101), (200), (111), (211), (220), (002), (310), (112), and (301) crystal planes of the tetragonal rutile structure with the space group $D_{4h}14$ (P_{42}/mnm), as referenced in JCPDS No. 21-1250. The positions of the diffraction peaks remain almost unchanged across different annealing temperatures, indicating that the crystalline structure of SnO_2 is stable under elevated temperatures. However, the intensity and sharpness of the peaks increase gradually with higher annealing temperatures. This enhancement suggests an increase in crystallite size and an improvement in crystallinity, which is attributed to thermally promoted crystallite growth and a reduction in specific surface area. The grain size of the crystallites and inter-planner spacing (d-value) were calculated based on Scherer's and Bragg's equations:

$$D = \frac{k\lambda}{\beta cos\theta} \text{ [10] and } d = \frac{\lambda}{2sin\theta} \text{ [11]}$$

where: D is the mean crystallite size, K is the shape factor taken as 0.89, λ is the wavelength of the incident beam, β is the full width at half maximum and θ is the Bragg angle. These results are shown in Table 1.

Table 1. XRD parameters and size of SnO_2 nanoparticles at different annealing temperatures.

Annealing temperature (°C)	2θ (°)	d- spacing (Å)	FWHM (°)	Crystallite size (nm)	Average crystalline size D (nm)
400	26.44	3.3687	1.2232	6.7	6.7
	33.70	2.6574	1.1681	7.1	
	51.67	1.7676	1.3842	6.4	
600	26.44	3.3683	1.0379	7.9	8.4
	33.71	2.6565	0.96572	8.6	
	51.65	1.7682	1.0200	8.7	
800	26.43	3.3701	0.82288	9.9	10.4
	33.72	2.6558	0.78625	10.6	
	51.65	1.7681	0.82315	10.7	
1100	26.48	3.3635	0.38631	21.1	20.3
	33.75	2.6536	0.40635	20.4	
	51.65	1.7679	0.44148	20.0	

Annealing at temperatures of 400 °C, 600 °C, 800 °C, and 1100 °C resulted in average grain sizes of 6.7, 8.4, 10.4 and 20.3 nm, respectively. Figure. 1(B) shows the typical TEM image of SnO_2 sample annealed at 600 °C. The TEM image depicts the irregular aggregated morphology. The SnO_2 nanoparticles are polyhedral or irregular in shape. The optimal annealing condition for SnO_2 samples depends on the desired application. For photocatalytic applications, smaller particle sizes are generally preferred because they increase the surface area for reactions, enhancing the photocatalytic activity. Thus, an annealing temperature range of 400 °C to 800 °C may be suitable.

Raman scattering is a useful technique for the characterizing of nanomaterials and identifying lattice defects in the materials [12]. Figure 2 shows the room temperature Raman spectra of SnO_2 nanoparticles annealed at different temperatures, ranging from 170 to 900 cm^{-1}. The positions and intensities of the Raman peaks vary significantly with annealing temperature. Notably, the intensity of the peak around 634 cm^{-1} increases rapidly as the annealing temperature rises. These changes may be related to the crystallite size and the crystalline quality of the synthesized SnO_2 [13]. At an annealing temperature of 1100 °C, the Raman spectrum of the sample exhibits nine peaks at 228, 259, 475, 506, 546, 634, 695, 776, and 866 cm^{-1}, with the strongest peak at 634 cm^{-1} (Figure. 2A). The peaks at 475, 634, and 776 cm^{-1} correspond to the E_g, A_{1g}, and B_{2g} vibration modes, respectively, consistent with the tetragonal rutile

structure [14]. The A_{1g} and B_{2g} modes are associated with the expansion and contraction of Sn-O bonds, while the E_g mode relates to oxygen vibrations within the oxygen plane [14]. Additionally, the peaks at 228 and 259 cm^{-1} may correspond to the $E_{u(1)}$(TO) and $E_{u(1)}$(LO) modes, where TO stands for transverse optical phonons and LO stands for longitudinal optical phonons [15, 16]. The peaks at 506 and 695 cm^{-1} may be attributed to the A_{2u}(TO) and A_{2u}(LO) modes, respectively [17]. The peak at 546 cm^{-1} may correspond to the B_{1u} mode [17], and the peak at 866 cm^{-1} is likely related to surface defects in the SnO_2 nanocrystals [18,19]. In contrast, samples annealed at 600 °C and 800 °C exhibit six peaks at 475 cm^{-1} (E_g), 634 cm^{-1} (A_{1g}), 774 cm^{-1} (B_{2g}), 253 cm^{-1} ($E_{u(1)}$(LO)), 301 cm^{-1} ($E_{u(2)}$(LO)) [15, 16], and 571 cm^{-1} (A_{2g}) [20] (Figure. 2B, C). At the lowest annealing temperature of 400 °C, the Raman spectrum shows seven broad and weak peaks at approximately 218, 268, 411, 537, 638, 758, and 870 cm^{-1}.

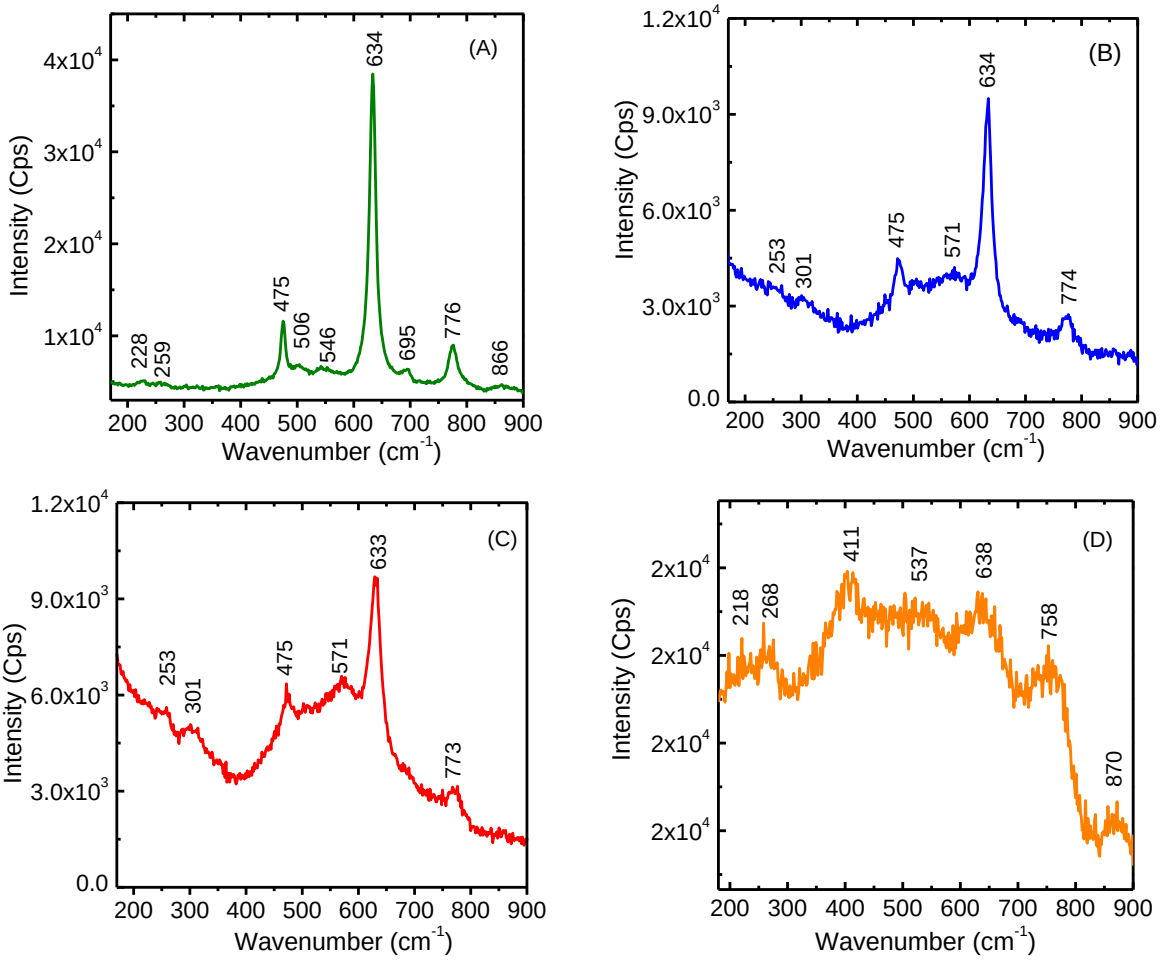

Figure 2. Raman spectra of SnO_2 samples at different annealing temperatures:
A- 1100 °C, B- 800 °C, C- 600 °C, D- 400 °C.

The peaks at 218, 268, and 758 cm^{-1} are attributed to the $E_{u(1)}$(TO), $E_{u(2)}$(LO), and $E_{u(3)}$(LO) vibrational modes of SnO_2, respectively [21]. The peaks at 411 and 537 cm^{-1} correspond to the A_{2g} [12] and B_{1u} [17] vibration modes. The peak at 638 cm^{-1} is attributed to the A_{1g} symmetric Sn–O stretching mode in nanocrystalline SnO_2, and the peak at 870 cm^{-1} is associated with surface defects [18, 19]. It is

well known that the A_{2u} and E_u modes are IR-active, while the A_{2g} and B_{1u} modes are Raman-silent [13-19]. The presence of forbidden Raman modes (A_{2g}, B_{1u}) and IR-active modes (A_{2u}, E_u) in the samples may be due to changes in bond lengths, reduced space symmetry, lattice distortions caused by oxygen vacancies, and local lattice disorders in the SnO_2 nanoparticles [19].

3.2. Optical Characterization

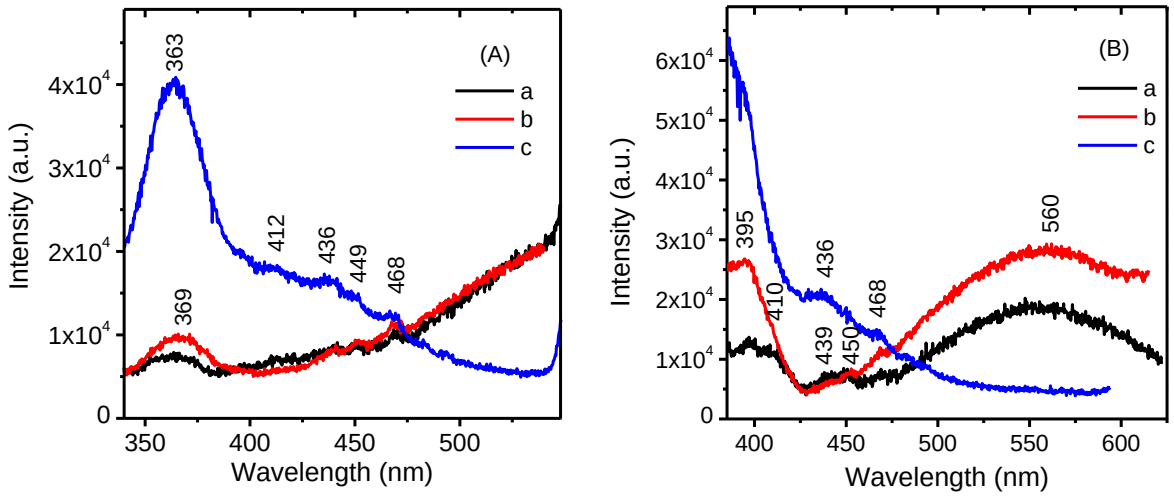

Figure 3. PL spectra under excitation wavelengths of (A) 300 nm and (B) 335 nm of the samples annealed at (a) 400 °C, (b) 800 °C and (c) 1100 °C.

Photoluminescence (PL) spectroscopy is a highly sensitive and effective technique for studying charge carrier recombination, trapping, and defects within materials. In SnO_2 nanoparticles, the most energetically favorable intrinsic defects are oxygen vacancies and tin interstitials. Tin interstitials are located within the conduction band, while oxygen vacancies exist in the band gap region [16]. PL spectra were recorded at two excitation wavelengths, λ_{ex} = 300 nm and λ_{ex} = 335 nm, for samples annealed at different temperatures, as shown in Figure. 3A and Figure. 3B, respectively. When excited at λ_{ex} = 300 nm, the sample annealed at 1100 °C exhibited a strong emission peak at 363 nm (3.42 eV) and four weaker peaks at 412 nm (3.01 eV), 436 nm (2.84 eV), 449 nm (2.76 eV), and 468 nm (2.65 eV). The samples annealed at 400 °C and 800 °C showed similar emission peaks but with significantly lower intensities compared to the 1100 °C sample. When excited at λ_{ex} = 335 nm, all samples displayed a new emission peak at approximately 395 nm (3.14 eV). Additionally, the samples annealed at 400 °C and 800 °C showed a broad emission band centered around 560 nm (2.21 eV). Emission peaks observed at 363 nm and 369 nm have energies lower than the band gap of SnO_2, indicating that these emissions are not due to the direct recombination of electrons in the conduction band with holes in the valence band. Instead, they are attributed to near-band edge (NBE) transitions resulting from the radiative recombination of electrons and holes [22]. The emission peak at 395 nm originated from the combination of the electron in the conduction band and the hole in the V_O^{++} (oxygen vacancy has not captured any electron) [23]. Another emission peak at 412 nm/410 nm was attributed to the V_O^0 (which has captured two electrons and is neutral to the lattice) [24]. The emission peak at 436 nm was attributed to the Sn interstitials [24]. The peak at 449 nm might be attributed to the transitions from the various levels of shallow donor states V_O^o to acceptor level [16]. The peak at 468 nm was attributed to the V_O^+ (which has

captured a single electron) [25]. Finally, the broad peak at 560 nm might be originating because of the transitions from the shallow donor levels of V_O^0 to the surface states and V_O^+ levels [16].

The photoluminescence spectra of the sample annealed at 800 °C were systematically examined under excitation wavelengths of 280 nm, 300 nm, 310 nm, 324 nm, and 335 nm (Figure. 4). Visible emission peaks at approximately 395 nm, 440 nm, 450 nm, and 468 nm, along with a broad peak around 560 nm, were consistently observed across all excitation wavelengths, with their intensities increasing as the excitation wavelength increased, aligning with previous studies on SnO_2 nanomaterials [23]. Additionally, the ultraviolet (UV) emission peaks shifted to longer wavelengths with higher excitation wavelengths, likely due to varying contributions from NBE emissions and their phonon replicas, resulting from recombination involving energy levels near the band gap [22, 25].

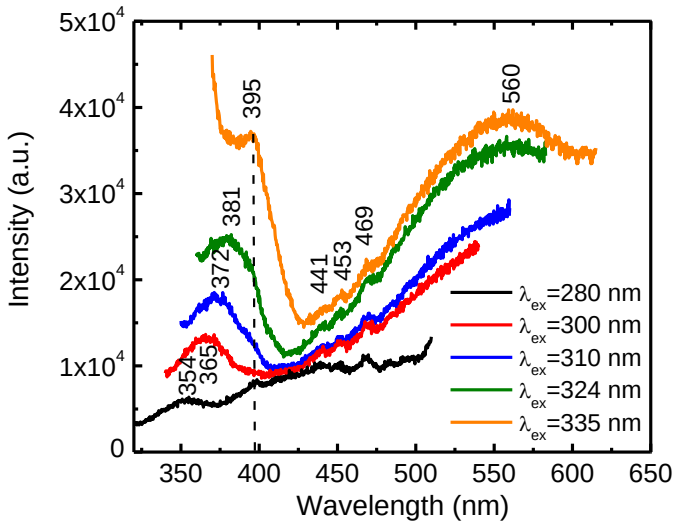

Figure 4. The excitation wavelength-dependent emission spectra of the samples annealed at 800 °C.

4. Conclusion

SnO_2 nanoparticles were successfully synthesized using a simple sol–gel method. This study investigated the effect of annealing temperature on the crystal structure and the origin of luminescence peaks in SnO_2 nanoparticles. X-ray diffraction (XRD) analysis revealed that all samples are polycrystalline, with diffraction lines corresponding to the tetragonal rutile phase of tin oxide. Both the crystallite size and crystal quality of the samples increased with higher annealing temperatures. These improvements in crystallite size and quality significantly enhanced the intensity of the A_{1g} vibration mode. Furthermore, some forbidden Raman and IR-active modes, such as A_{2g}, B_{1u}, A_{2u}, and E_u, which are inactive in bulk samples, became active in the SnO_2 nanoparticles. Photoluminescence (PL) spectra exhibited peaks in both the ultraviolet (UV) and visible regions. Visible emission peaks correspond to the V_O^0, V_O^+, V_O^{++} and the Sn interstitials in SnO_2 nanoparticles. The existence of oxygen vacancies and Sn interstitials in the sample annealing temperature range of 400 °C to 800 °C creates defect energy levels within the band gap, effectively reducing the energy required for electrons to transition across the gap. This phenomenon can improve the material's solar light absorption and utilization. This research provides valuable foundational knowledge that will support future studies on SnO_2.

References

[1] I. E. Kolesnikov, D. S . Kolokolov, M. A. Kurochkin, M. A. Voznesenskiy, M. G. Osmolowsky, E. Lähderanta, O. M. Osmolovskaya, Morphology and Doping Concentration Effect on the Luminescence Properties of SnO_2:Eu^{3+} nanoparticles, J. Alloys Compd., Vol. 822, No. 15340, 2020, https://doi.org/10.1016/j.jallcom.2020.153640.

[2] D. Toloman, A. Popa, M. Stefan, T. D. Silipas, R. C. Suciu, L. B. Tudoran, O. Pana, Enhanced Photocatalytic Activity of Co Doped SnO_2 Nanoparticles by Controlling the Oxygen Vacancy States, Optical Materials, Vol. 110, No. 110472, 2020, https://doi.org/10.1016/j.optmat.2020.110472.

[3] A. Wang, K. Bushick, N. Pant, W. Lee, X. Zhang, J. Leveillee, F. Giustino, S. Poncé, E. Kioupakis, Electron Mobility of SnO_2 from First Principles, Appl. Phys. Lett., Vol. 124, No. 172103, 2024, https://doi.org/10.1063/5.0198885.

[4] Y. Kong, Z. Ma, Y. Ye, G. He, Y. Sun, X. Zuo, X. Xiao, and J. Nan, Nanosized Amorphous SnO_2 Particles Anchored in the Wheat Straw Carbon Substrate as the Stabilized Anode Material of Lithium-Ion Batteries, ACS Appl. Energy Mater., Vol. 1, No. 12, 2018, pp. 7065-7075, https://doi.org/10.1021/acsaem.8b01408.

[5] N. N. Dinh, M. C. Bernard, A. H. Goff, T. Stergiopoulos, P. Falaras, Photoelectrochemical Solar Cells Based on SnO_2 Nanocrystalline Films, C.R. Chimie, Vol. 9, No. 5-6, 2006, pp. 676-683, https://doi.org/10.1016/j.crci.2005.02.042.

[6] G. Ramanathan, K. R. Murali, Photocatalytic Activity of SnO_2 Nanoparticles, J. Appl. Electrochem., Vol. 52, 2022, pp. 849-859, https://doi.org/10.1007/s10800-022-01676-z.

[7] J. H. Lee, Y. J. You, M. A. Saeed, S. H. Kim , S. H. Choi, S. Kim, S. Y. Lee, J. S. Park, J. W. Shim, Undoped tin Dioxide Transparent Electrodes for Efficient and Cost-Effective Indoor Organic Photovoltaics (SnO_2 Electrode for Indoor Organic Photovoltaics), NPG Asia Mater, Vol. 13, No. 43, 2021, pp. 1-10, https://doi.org/10.1038/s41427-021-00310-2.

[8] Y. Kong, Y. Li, X. Cui, L. Su, D. Ma, T. Lai, L. Yao, X. Xiao, Y. Wang, SnO_2 Nanostructured Materials Used as Gas Sensors for the Detection of Hazardous and Flammable Gases: A review, Nano Materials Science, Vol. 4, No. 4, 2022, pp. 339-350, https://doi.org/10.1016/j.nanoms.2021.05.006.

[9] R. Ponte, E. Rauwel, P. Rauwel, Tailoring SnO_2 Defect States and Structure: Reviewing Bottom-Up Approaches to Control Size, Morphology, Electronic and Electrochemical Properties for Application in Batteries, Materials, Vol. 16, No. 12, 2023, https://doi.org/10.3390/ma16124339.

[10] B. D. Cullity, S. R. Stock, Elements of X-Ray Diffraction, 3rd Ed., Prentice-Hall Inc., ISBN 0-201-61091-4.2001, pp. 96-102.

[11] W. L. Bragg, The Reflection of X-rays by Crystals, Proceedings of the Royal Society of London, Series A, Vol. 89, No. 611, 1913, pp. 482-493.

[12] N. Haddad, Z. B. Ayadi, H. Mahdhi, K. Djessas, Influence of Fluorine Doping on the Microstructure, Optical and Electrical Properties of SnO_2 Nanoparticles, J. Mater. Sci.: Mater Electron, Vol. 28, 2017, pp. 15457-15465, https://doi.org/10.1007/s10854-017-7433-1.

[13] J. Zuo, C. Xu, X. Liu, C. Wang, C. Wang, Y. Hu, Y. Qian, Study of the Raman Spectrum of Nanometer SnO_2, J. Appl. Phys., Vol. 75, No. 3, 1994, pp. 1835-1836, https://doi.org/10.1063/1.356348.

[14] S. Sambasivam, I. M. Obaidat, Effect of Iron Doping on ESR and Raman Spectra of SnO_2 Nanomaterials, Materials Today: Proceedings, Vol. 28, 2020, pp. 587-590, https://doi.org/10.1016/j.matpr.2019.12.225.

[15] N. Ahmad, S. Khan, M. M. N. Ansari, Exploration of Raman Spectroscopy, Dielectric and Magnetic Properties of (Mn, Co) Co-doped SnO_2 Nanoparticles, Phys. Rev. B Condens. Matter., Vol. 558, 2019, pp. 131-141, https://doi.org/10.1016/j.physb.2019.01.044.

[16] S. Roy, A. G. Joshi, S. Chatterjee, A. K. Ghosh, Local Symmetry Breaking in SnO_2 Nanocrystals with Cobalt Doping and Its Effect on the Optical Properties, Nanoscale, Vol. 10, No. 22, 2018, pp. 10664-10682, https://doi.org/10.1039/C7NR07427A.

[17] L. Abello, B. Bochu, A. Gaskov, S. Koudryavtseva, G. Lucazeau, M. Roumyantseva, Structural Characterization of Nanocrystalline SnO_2 by X-Ray and Raman Spectroscopy, J. Solid State Chem., Vol. 135, No. 1, 1998, pp.78-85. https://doi.org/10.1006/jssc.1997.7596.

[18] N. Bhardwaj, S. Kuriakose, S. Mohapatra, Structural and Optical Properties of SnO_2 Nanotowers and Interconnected Nanowires Prepared by Carbothermal Reduction Method, J. Alloys Compd, Vol. 592, No. 15, 2014, pp. 238-243, https://doi.org/10.1016/j.jallcom.2013.12.268.

[19] W. B. H. Othmen, B. Sieber, H. Elhouichet, A. Addad, B. Gelloz, M. Moreau, S. Szunerits, R. Boukherroub, Effect of High Fe Doping on Raman Modes and Optical Properties of Hydrothermally Prepared SnO_2 Nanoparticles, Materials Science in Semiconductor Processing, Vol. 77, 2018, pp. 31-39, https://doi.org/10.1016/j.mssp.2017.12.014.

[20] V. Bonu, A. Das, A. K. Sivadasan, A. K. Tyagi, S. Dhara, Invoking Forbidden Modes in SnO_2 Nanoparticles Using Tip Enhanced Raman Spectroscopy, J. Raman Spectrosc, Vol. 46, No. 11, 2015, pp. 1037-1040, https://doi.org/10.1002/jrs.4747.

[21] A. Diéguez, A. R. Rodríguez, A. Vilà, J. R. Morante, The Complete Raman Spectrum of Nanometric SnO_2 Particles. J. Appl. Phys., Vol. 90, No. 3, 2001, pp. 1550-1557, https://doi.org/10.1063/1.1385573.

[22] R. Mani, K. Vivekanandan, K. Vallalperuman, Synthesis of Pure and Cobalt (Co) Doped SnO_2 Nanoparticles and its Structural, Optical and Photocatalytic Properties, J Mater Sci: Mater Electron, Vol. 28, No. 5, 2017, pp. 4396-4402, https://doi.org/10.1007/s10854-016-6067-z.

[23] M. Xu, X. Ruan, J. Yan, Z. Zhang, J. Yun, W. Zhao, T. Li, Y. Shi, Synthesis, Growth Mechanism, and Photoluminescence Property of Hierarchical SnO_2 Nanoflower-rod Arrays: an Experimental and First Principles Study, J. Mater. Sci., Vol. 51, No. 21, 2016, pp. 9613-9624, https://doi.org/10.1007/s10853-016-0169-0.

[24] H. Sefardjella, B. Boudjema, A. Kabir, G. Schmerber, Structural and Photoluminescence Properties of SnO_2 Obtained by Thermal Oxidation of Evaporated Sn Thin Films, Current Applied Physics, Vol. 13, No. 9, 2013, pp. 1971-1974, https://doi.org/10.1016/j.cap.2013.08.017.

[25] I. L. P. Raj, M. S. Revathy, A. J. Christy, N. Chidhambaram, V. G. S. AlFaify, Study on the Synergistic Effect of Terbium-doped SnO_2 Thin Film Photocatalysts for Dye Degradation, J. Nanopart. Res., Vol. 22, No. 359, 2020, https://doi.org/10.1007/s11051-020-05084-2.